Evidence for tidal triggering of earthquakes as revealed from statistical analysis of global data

Sachiko Tanaka, Masakazu Ohtake, and Haruo Sato

Department of Geophysics, Graduate School of Science, Tohoku University, Sendai, Japan

Received 16 October 2001; revised 24 March 2002; accepted 29 March 2002; published 5 October 2002.

[1] We observe tidal triggering of earthquakes by measuring the correlation between the Earth tide and earthquake occurrence. We used the times, locations, and focal mechanisms of the 9350 globally distributed earthquakes with magnitude 5.5 or larger from the Harvard centroid moment tensor catalog. The tidal stress was theoretically computed by using the Preliminary Reference Earth Model and a recent ocean tide model, NAO.99b. We considered the shear stress on the fault plane and the trace of stress tensor, J1. Defining the tidal phase angle at the occurrence time for each earthquake, we statistically tested the phase selectivity using the Schuster's method. For all the earthquakes, no significant correlation is found between the Earth tide and earthquake occurrence both for the shear stress and for J1. By classifying the data set according to fault types, however, we find a high correlation with the shear stress for reverse fault type. The correlation is particularly clear for shallow and smaller earthquakes of this type. Significant correlation with J1 also appears for larger earthquakes of reverse fault type and for shallow and larger ones of normal fault type. We find no correlation for strike-slip type. For all the cases of high correlation, earthquakes tend to occur when the tidal stress accelerates the fault slip, indicating that high correlation is not coincidental but is physically justified. This result strongly suggests that a small stress change due to the Earth tide encourages earthquake occurrence when the stress in the future focal area is near a critical condition. *INDEX TERMS:* 7230 Seismology: Seismicity and seismotectonics; 1249 Geodesy and Gravity: Tides—Earth; 7223 Seismology: Seismic hazard assessment and prediction; 7209 Seismology: Earthquake dynamics and mechanics; 1223 Geodesy and Gravity: Ocean/Earth/atmosphere interactions (3339); *KEYWORDS:* tidal triggering, statistical test, Earth tide, ocean loading, Harvard CMT catalog

Citation: Tanaka, S., M. Ohtake, and H. Sato, Evidence for tidal triggering of earthquakes as revealed from statistical analysis of global data, *J. Geophys. Res.*, *107*(B10), 2211, doi:10.1029/2001JB001577, 2002.

1. Introduction

[2] The stresses due to the Earth tide oscillate and are superimposed on tectonic stresses. Although the amplitude of the tidal stress change, of order 10^3 Pa, is much smaller than the average stress drop of earthquakes, its rate is generally larger than that of tectonic stress accumulation. Therefore tidal triggering of earthquakes may be expected when the stress in the focal area is near the critical level to release an earthquake. Measuring tidal triggering may give us a clue to solve the physical mechanism of initiation of fault rupture. Since we can predict the stress change due to the Earth tide, there have been numerous searches for the relation between the Earth tide and earthquake occurrence.

[3] Most studies with global catalogs have reported no correlation between the Earth tide and earthquake occurrence [*Schuster*, 1897; *Morgan et al.*, 1961; *Simpson*, 1967; *Heaton*, 1982; *Curchin and Pennington*, 1987; *Hartzell and Heaton*, 1989] with few exceptions [*Heaton*, 1975; *Ding et al.*, 1983; *Tsuruoka et al.*, 1995]. Regional catalogs have also been investigated; a significant correlation has been reported by some studies [*Young and Zurn*, 1979; *Ulbrich et al.*, 1987; *Shirley*, 1988], but no correlation by some other studies [*Knopoff*, 1964; *Shlien*, 1972; *Shudde and Barr*, 1977; *Vidale et al.*, 1998]. On the other hand, an especially high correlation has been found for aftershock sequences [*Berg*, 1966; *Ryall et al.*, 1968; *Mohler*, 1980; *Souriau et al.*, 1982], earthquake swarms [*Sauck*, 1975; *Klein*, 1976; *Rykunov and Smirnov*, 1985; *Oike and Taniguchi*, 1988], and earthquakes occurring in volcanic areas [*McNutt and Beavan*, 1984; *Rydelek et al.*, 1988]. *Emter* [1997] gives an elaborate review of past studies.

[4] At first, lunar and solar periodicities were sought in the time series of earthquake occurrence [*Schuster*, 1897; *Morgan et al.*, 1961]. In the following studies, the earthquake occurrence times were related to theoretical time functions of tidal changes, which include the tidal potential [*Shlien*, 1972; *Shirley*, 1988], gravity [*Knopoff*, 1964; *Simpson*, 1967; *Sauck*, 1975; *Shudde and Barr*, 1977; *Rykunov and Smirnov*, 1985], and strain [*Klein*, 1976; *Young and Zurn*, 1979; *McNutt and Beavan*, 1984; *Oike and Taniguchi*, 1988; *Rydelek et al.*, 1988]. However, the most likely component to control the earthquake occurrence is the stress, and the

0148-0227/02/2001JB001577$09.00

relation between the stress and such tidal components is complicated. Therefore these studies have difficulty relating the Earth tide with the physical mechanism of fault rupture. The best way is to examine the tidal stress in relation to the fault plane. Another problem is that the theoretical Earth tide was calculated for the ground surface, not for the depth of earthquake occurrence in most studies.

[5] *Heaton* [1975] was the first study that considered the stress change on the fault plane of each earthquake taking the focal depth in consideration. He analyzed a global catalog of 107 earthquakes and found a significant correlation between the shear stress in the slip direction and earthquake occurrence time for a subset of 34 shallow earthquakes with dip-slip and oblique-slip faulting. After this study, the stress change on the fault plane was considered in the investigations of *Mohler* [1980], *Heaton* [1982], *Ding et al.* [1983], and *Ulbrich et al.* [1987]. *Heaton* [1982] examined again a global catalog updated to 328 earthquakes and reached the opposite conclusion from his earlier study. No correlation was found for the new data set. However, there remained a problem that the indirect term of the Earth tide, that is, the effect of ocean loading, was ignored in these studies.

[6] The Earth tide is composed of two components; the direct term that is produced by the traction force of the Moon and the Sun, and the indirect term that is produced by the ocean tide. Near ocean margins, the effect of indirect term is sometimes much larger than that of direct term, with considerable phase shift. Therefore neglecting the indirect term may lead to erroneous conclusions. *Tsuruoka et al.* [1995] solved this problem, incorporating the indirect term into the calculation of the tidal stress. They analyzed 988 globally distributed earthquakes and found a significant correlation for normal fault type earthquakes. The effect of ocean loading was also considered by *Souriau et al.* [1982] and *Vidale et al.* [1998], but *Souriau et al.* [1982] used the stress at the ground surface again.

[7] Few studies have carefully investigated the relation between the Earth tide and earthquake occurrence; some studies ignored the effect of the ocean loading, and some studies used the tidal stress at the ground surface for analysis. Therefore the resolution of analysis in most studies may be lost. These problems are basically solved by *Tsuruoka et al.* [1995], but this study still leaves two weak points; the ocean tide model to compute the indirect term was not reliable enough, and the number of earthquakes that they analyzed was rather small to obtain clear result.

[8] In this paper, we investigate the relation between the Earth tide and earthquake occurrence following the method of *Tsuruoka et al.* [1995] but improve it in the above two points. First, the ocean tide model to compute the indirect term is changed from a conventional model of *Schwiderski* [1980] to a recent one, NAO.99b [*Matsumoto et al.*, 2000; *Takanezawa et al.*, 2001], which was constructed by using the satellite altimetry data. This leads to more realistic estimates of the tidal stress. Second, the number of the earthquake data is increased by nearly ten times to secure statistical reliability.

2. Theoretical Earth Tide

[9] We compute the deformation of solid earth due to the tidal force (direct term) and that due to the ocean loading (indirect term). The effect of ocean loading is computed by the convolution of the ocean tide model and the Green's functions defined by the deformation due to the unit point mass acting on the Earth's surface. In this convolution, we use a recent ocean tide model, NAO.99b [*Matsumoto et al.*, 2000; *Takanezawa et al.*, 2001] to obtain sufficiently high accuracy in the calculation.

[10] We assume that the Earth is spherically symmetric, nonrotating, self-gravitating, elastic and isotropic, and that it is initially in a hydrostatic equilibrium state. Lateral heterogeneity of the Earth is ignored for simplicity. The deformation of this Earth due to the tidal force or the surface mass loading can be represented in terms of spherical harmonics with six variables depending on radius and degree n [*Alterman et al.*, 1959]. These spherical harmonics are associated with the potential of the exerted force. On the other hand, the six variables are governed by a system of six ordinary differential equations of first order for each degree [*Takeuchi and Saito*, 1972; *Saito*, 1974]. Different boundary conditions are imposed at the Earth's surface for the tidal force and the surface mass loading. To solve this system, we perform numerical integration with a fourth-order Runge-Kutta scheme. We take the step size as less than one-hundredth of a wavelength to obtain a stable numerical solution. The Earth model we use is the same as that used by *Tsuruoka et al.* [1995]; the isotropic Preliminary Reference Earth Model (PREM) [*Dziewonski and Anderson*, 1981] with a slight modification, in which the top oceanic layer with thickness of 3 km is replaced by a solid layer of P wave velocity of 5 km/s, S wave velocity 2.6 km/s, and density 2.6 g/cm^3.

[11] To compute the direct term, we consider the Moon and the Sun as celestial bodies producing the tidal effect on the Earth. When the tidal potential is expanded into a series of spherical harmonics, the solution can be sufficiently expressed only by the term of degree 2 both for the Moon and the Sun. We obtain the direct term by summing them.

[12] On the other hand, the potential of surface mass loading can also be represented by infinite sum of spherical harmonics in terms of degree n [*Longman*, 1962; *Farrell*, 1972], but it is not sufficient to consider low degrees only. Following *Farrell* [1972], we sum the terms up to n = 10,000 in order to obtain the Green's functions of the indirect term, which secures a spatial resolution better than 2 km. The indirect term is obtained by the convolution of the ocean tide model and these Green's functions.

[13] Today, because of the availability of high-resolution satellite altimetry data, many ocean tide models are available and their accuracy has been significantly improved in the open sea. Using the data of 5 years, *Matsumoto et al.* [2000] developed a global ocean tide model (NAO.99b) and a regional one around Japan (NAO.99Jb) for 16 major constituents in short-period bands (M2, S2, K1, O1, N2, P1, K2, Q1, M1, J1, OO1, 2N2, Mu2, Nu2, L2, T2). *Takanezawa et al.* [2001] also developed a long-period global model (NAO.99L) for five constituents (Mtm, Mf, Mm, Ssa, Sa) by using purely hydrodynamic computation. The resolution of these models is 0.5° for NAO.99b and NAO.99L, and as high as 5′ for NAO.99Jb. For the computation of loading effect, many studies, such as *Tsuruoka et al.* [1995], have used *Schwiderski*'s [1980] model as a conventional ocean tide model, but we use more accurate models, NAO.99b, NAO.99Jb and NAO.99L. *Shum et al.* [2001] confirmed that these are the most reliable of the recent ones. In the present

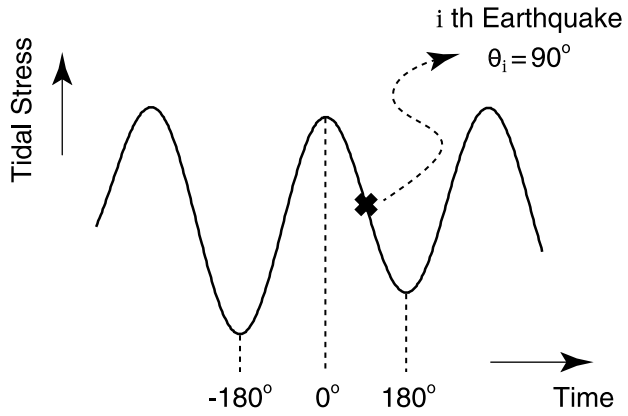

Figure 1. Definition of tidal phase angle. The maximum and the minimum of the tidal stress just before or after each earthquake are assigned to 0° and ±180°, respectively, and the tidal phase angle is defined by linearly dividing the time interval between them.

study, we compute the ocean load distribution by integrating the new models, which are referred to together as NAO.99b hereinafter.

[14] In the convolution of the ocean tide model and the Green's functions, we divide the ocean regions into small rectangular cells, following a program for computation of oceanic tidal loading effect, GOTIC2 [*Matsumoto et al.*, 2001]. The cell size is $0.5° \times 0.5°$ for $\Theta > 10°$, $7.5' \times 7.5'$ for $5° < \Theta \leq 10°$ and $45'' \times 45''$ for $\Theta \leq 5°$, where Θ is the angular distance from the loading point. This secures a spatial resolution better than 10 km, which is comparable to the resolution for the Green's functions.

3. Method of Statistical Test

[15] We statistically test a correlation between the Earth tide and earthquake occurrence using the Schuster's test, following *Heaton* [1975, 1982], *Tsuruoka et al.* [1995], and many other studies.

[16] First, we assign the tidal phase angle at the occurrence time of each earthquake. The phase angle is measured from the time series of the tidal stress, which is calculated at the location of the hypocenter, including both the direct and indirect terms as described in the previous section. The tidal phase angle θ_i, taking a value between $-180°$ and $180°$ is defined for the ith earthquake as illustrated in Figure 1. The value is assigned by linearly dividing the time interval from 0° to 180° or from $-180°$ to 0°, where 0° and ±180° corresponds to the maximum and the minimum of the tidal stress immediately before or after each earthquake occurrence, respectively.

[17] Determining the phase angles for all the earthquakes in a data set, we statistically test whether they concentrate near some particular angle or not by using the Schuster's test. In the Schuster's test, each earthquake is represented by a unit length vector in the direction defined by its tidal phase angle. The length of the vectorial sum D is defined as

$$D^2 = \left(\sum_{i=1}^{N} \cos\theta_i\right)^2 + \left(\sum_{i=1}^{N} \sin\theta_i\right)^2, \quad (1)$$

where θ_i is the phase angle of the ith earthquake and N is the total number of the earthquakes included in the data set. When θ_i ($i = 1, 2, \ldots, N$) distribute randomly, the probability that the length of a vectorial sum is equal to or larger than D is given by

$$p = \exp\left(-\frac{D^2}{N}\right). \quad (2)$$

Thus the p value represents the significance level to reject the null hypothesis that the earthquakes occur randomly irrespective of the phase angle. The p value ranges between 0 and 1, and the smaller the p value is, the higher the confidence in rejecting the null hypothesis is. In the present study, we tentatively adopt a threshold of $p < 5\%$ to judge a significant correlation between the Earth tide and earthquake occurrence.

4. Analysis and Result

4.1. Data and Stress Components

[18] We use 9350 globally distributed earthquakes with moment magnitude (M_w) 5.5 or larger, which are listed in the Harvard centroid moment tensor (CMT) catalog for the period from 1977 to 2000. Figure 2 shows the magnitude distribution of the earthquakes listed in the CMT catalog. Although small-sized earthquakes escape the catalog, $M_w \geq 5.5$ events are expected to be completely covered judging from the magnitude-frequency distribution. From the catalog, we use the centroid location, origin time, and focal mechanism of the best double-couple solution for each earthquake. Figure 3 shows the epicentral distribution of the earthquakes that we analyze.

[19] The most important tidal components to affect the fault rupture are the normal stress and the shear stress on the fault plane. We examine the shear stress along the slip direction on the fault plane. However, we do not use the normal stress because it is difficult to identify the fault plane from the two nodal planes. Because of the symmetry of the

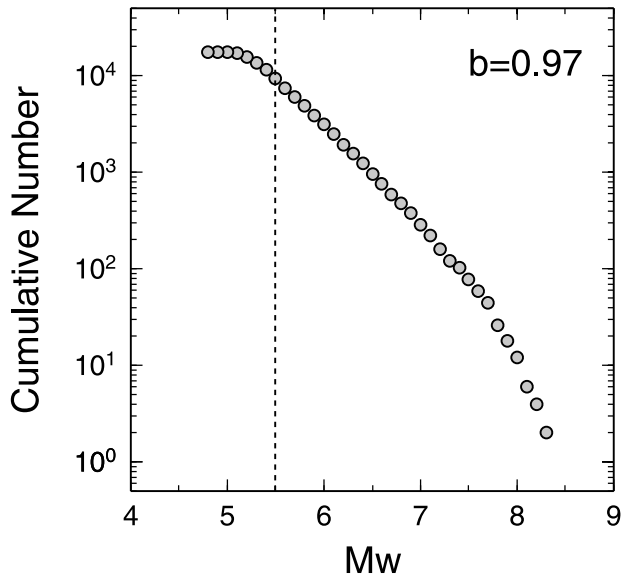

Figure 2. Cumulative frequency of earthquake magnitude listed in the Harvard CMT catalog for the period from 1977 to 2000.

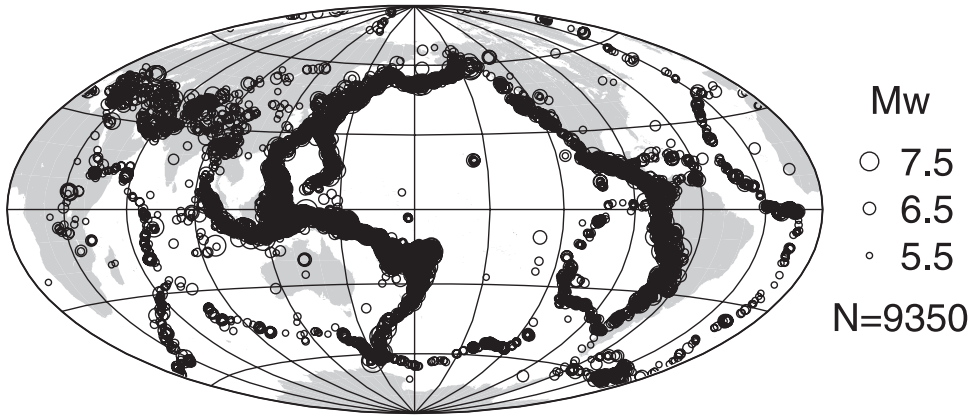

Figure 3. Epicentral distribution of 9350 earthquakes used in the present study.

stress tensor, the shear stress does not depend on the selection of the fault plane. We also examine the trace of stress tensor, J1, which represents confining stress and is invariant with coordinate rotation. The sign of stress change is defined as follows. The shear stress is positive when it is in the same sense as the fault slip so that the phase angle 0° means the maximum stress in the slip direction (see Figure 1). For J1, tension is positive so that 0° and ±180° correspond to the maximum tensional stress and the maximum compressional stress, respectively.

4.2. Result

[20] Figure 4 shows the results of analysis using all the earthquakes for the shear stress and for J1. The histogram is the frequency distribution of phase angles, in which earthquakes are gathered into phase angle windows of 30° width. The sinusoidal curve shows the least squares fitting of

$$P(\theta) = P_0 + P_1 \cos(\theta - \phi) \tag{3}$$

to the frequency distribution, where θ is the phase angle, P_0 is the mean frequency, P_1 and ϕ are the amplitude and phase of the fitted curve, respectively. The p value obtained by the Schuster's test and the total number of earthquakes included in the data set are also provided at the top right of each histogram. In Figure 4, the frequency distribution is nearly flat both for the shear stress and for J1, and the p value is as large as 77% and 9.5%. This means that there is no correlation for the data set including all the earthquakes distributed all over the world.

[21] Next, we classify the data into four subsets following their fault types; reverse, normal, strike-slip and oblique-slip faults. The classification of fault types is shown in Table 1. As is shown in Table 1, about 30% of the earthquakes are not classified into the four categories since the fault type depends on the selection of fault plane from two nodal planes. Excluding these unclassified cases, the number of earthquakes totals 6555. Figure 5 shows the results for the shear stress. An extremely high correlation appears for reverse fault type; p value is as small as 0.04%. In the case of $p < 5\%$ the peak of the phase angle distribution is shown by a triangle in the histogram. In Figure 5a, the value of ϕ in equation (3), which represents the phase angle at the peak of the distribution, is $-49°$, and its histogram shows that many earthquakes tend to occur a little before the shear stress in the slip direction reaches at the maximum. We find no correlation for other fault types. The results for J1 are shown in Figure 6, but a significant correlation is not found for any fault types.

[22] We further classify the earthquakes into two categories according to the focal depth; shallow earthquakes (focal depth < 70 km) and deep ones (focal depth $\geq$ 70 km). The statistical results for these two categories are shown in Table 2. The case of $p < 5\%$ is indicated in Table 2. For the shear stress, a small p value is again obtained for shallow earthquakes of reverse fault type ($p = 0.20\%$). On the other hand, a significant correlation is not found for any cases of J1.

[23] Furthermore, we divide each data set into four groups according to earthquake magnitude: $5.5 \leq M_w \leq 6.4$, $6.0 \leq M_w \leq 6.9$, $6.5 \leq M_w \leq 7.4$, and $7.0 \leq M_w \leq 7.9$.

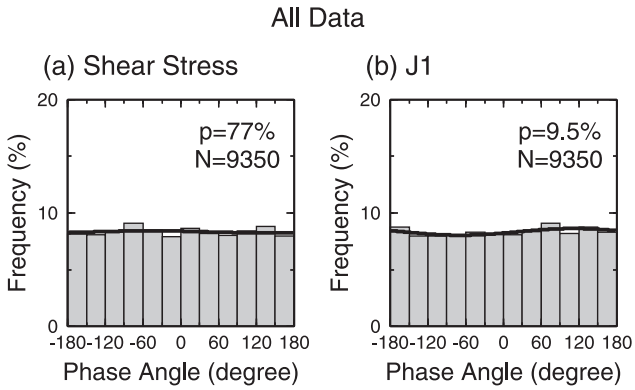

Figure 4. Frequency distributions of tidal phase angles for all the earthquakes: (a) the shear stress, (b) J1. Solid curve represents a sinusoidal function fitted to the distribution.

Table 1. Classification of Fault Types

Fault Type	N	Slip Direction
Reverse	2823	$60° \leq$ rake $\leq 120°$
Normal	1040	$-120° \leq$ rake $\leq -60°$
Strike-slip	2145	$0° \leq \lvert\text{rake}\rvert \leq 30°$, $150° \leq \lvert\text{rake}\rvert \leq 180°$
Oblique	547	$30° < \lvert\text{rake}\rvert < 60°$, $120° < \lvert\text{rake}\rvert < 150°$
Not classified	2795	
Total	9350	

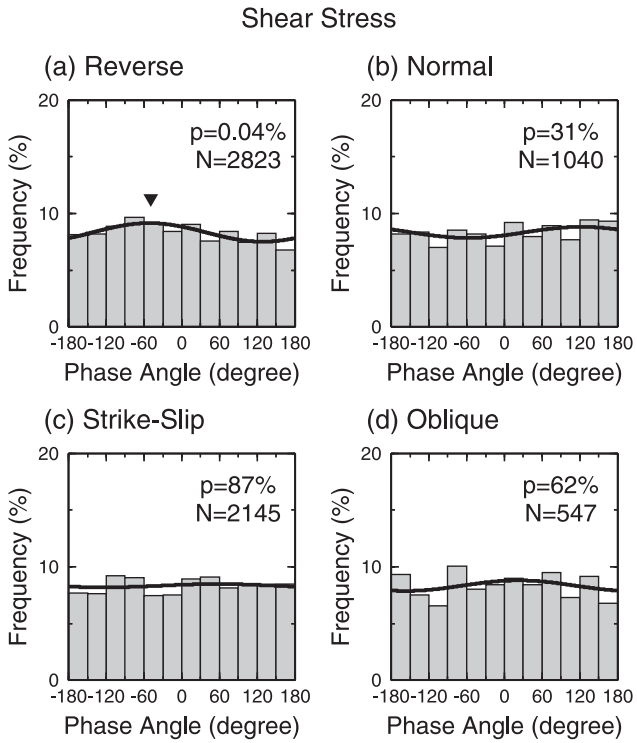

Figure 5. Frequency distributions of tidal phase angles for the shear stress. The four histograms are for different fault types: (a) reverse, (b) normal, (c) strike-slip, and (d) oblique type. Solid curve represents a sinusoidal function fitted to the distribution, of which peak is indicated by a triangle for the case of $p < 5\%$.

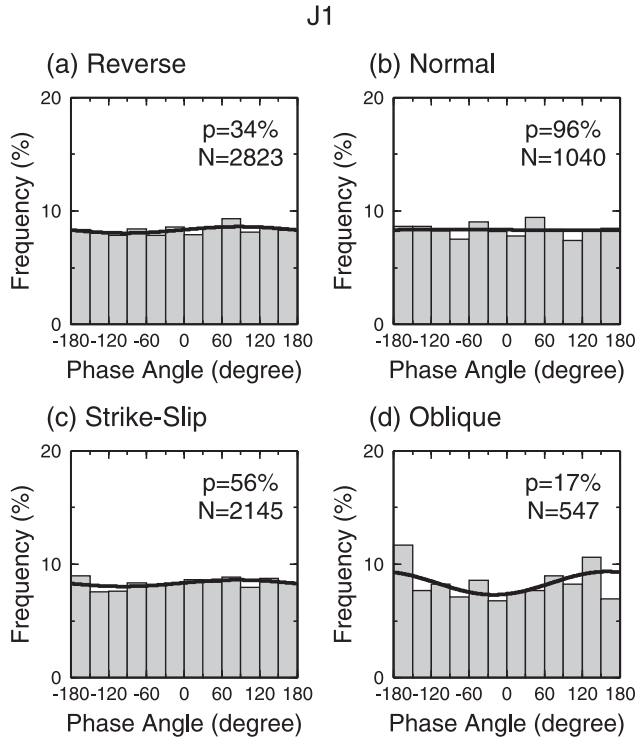

Figure 6. Frequency distributions of tidal phase angles for J1. The four histograms are for different fault types: (a) reverse, (b) normal, (c) strike-slip, and (d) oblique type. Solid curve represents a sinusoidal function fitted to the distribution.

Magnitude windows are overlapped to keep sufficient number of earthquakes. The results for earthquakes including both shallow and deep ones are shown in Table 3. Small p values are obtained only for reverse fault type earthquakes. The frequency distributions of phase angles for reverse fault type are shown in Figure 7. For the shear stress, small p values appear for $5.5 \leq M_w \leq 6.4$ ($p = 0.19\%$) and for $6.0 \leq M_w \leq 6.9$ ($p = 4.9\%$). The peak of smoothed distribution appears at $\phi = -58°$ for $5.5 \leq M_w \leq 6.4$ and $\phi = -22°$ for $6.0 \leq M_w \leq 6.9$. For J1, a small p value is found for larger earthquakes, $7.0 \leq M_w \leq 7.9$ ($p = 2.1\%$) with a peak near the phase angle $\pm 180°$ ($\phi = 167°$), which corresponds to the maximum compressional stress.

[24] The statistical results for shallow earthquakes are shown in Table 4. Small p values appear for reverse, normal and oblique faults but do not for strike-slip type. For reverse fault type, the cases of $p < 5\%$ are the shear stress for $5.5 \leq M_w \leq 6.4$ ($p = 0.68\%$), and J1 for $7.0 \leq M_w \leq 7.9$ ($p = 4.2\%$). Figure 8 shows the frequency distributions of phase angles for these two cases. The peak of the phase angle distribution is at $\phi = -54°$ for Figure 8a and $\phi = 175°$ for Figure 8b, which is very near the maximum compressional stress. Small p values are also obtained for normal fault type; J1 for $6.0 \leq M_w \leq 6.9$ ($p = 2.1\%$) and $6.5 \leq M_w \leq 7.4$ ($p = 3.8\%$). Figure 9 shows the frequency distributions of phase angles for these two cases. The phase angles concentrate near 0°; $\phi = -9°$ for $6.0 \leq M_w \leq 6.9$ and $\phi = -37°$ for $6.5 \leq M_w \leq 7.4$. This means that many earthquakes tend to occur near the maximum tensional stress. For oblique-slip type, a small p value appears only for the shear stress of $5.5 \leq M_w \leq 6.4$ earthquakes. For strike-slip type, we find no correlation in any cases.

[25] Table 5 shows the results for deep earthquakes. Small p values are obtained for reverse fault type earthquakes of $6.0 \leq M_w \leq 6.9$ both for the shear stress ($p = 4.0\%$) and J1 ($p = 0.40\%$), and for normal fault type earthquakes of $6.0 \leq M_w \leq 6.9$ for the shear stress ($p = 3.4\%$). Again such a high correlation is not seen for strike-slip earthquakes.

Table 2. Results of Schuster's Test for Shallow and Deep Earthquakes

Fault Type	N	p, %	
		Shear Stress	J1
	Shallow Depth[b]		
Reverse	2560	0.20[a]	17
Normal	713	19	63
Strike-slip	2010	88	41
Oblique	303	88	62
	Deep Depth[c]		
Reverse	263	12	9.5
Normal	327	82	20
Strike-slip	135	72	32
Oblique	244	51	13

[a] $p < 5\%$.
[b] Focal depth < 70 km.
[c] Focal depth ≥ 70 km.

Table 3. Results of Schuster's Test for Various Ranges of Earthquake Magnitude

M_w	N	p, %	
		Shear Stress	J1
	Reverse Fault		
5.5–6.4	2467	0.19[a]	14
6.0–6.9	915	4.9[a]	72
6.5–7.4	320	6.8	17
7.0–7.9	118	5.3	2.1[a]
	Normal Fault		
5.5–6.4	932	30	92
6.0–6.9	307	25	14
6.5–7.4	102	73	38
7.0–7.9	28	13	8.7
	Strike-Slip Fault		
5.5–6.4	1985	87	27
6.0–6.9	676	94	60
6.5–7.4	147	88	28
7.0–7.9	36	9.3	24
	Oblique Fault		
5.5–6.4	501	51	6.6
6.0–6.9	126	92	30
6.5–7.4	44	99	54
7.0–7.9	11	66	32

[a] $p < 5\%$.

[26] In Table 6, we summarize the results for various kinds of data subsets, classified by fault types, focal depth and earthquake magnitude. A circle indicates the case in which $p < 5\%$ appears for some magnitude range(s). A cross indicates the other. For reverse fault type earthquakes, the correlation between the Earth tide and earthquake occurrence is the most remarkable. For normal fault type, significant correlations appear in some cases. On the other hand, we find no correlation for strike-slip type. Surveying the cases of small p values ($p < 5\%$), we find a remarkable regularity in the phase angle of the peak frequency ϕ. For the shear stress, ϕ, ranging between $-58°$ and $-22°$, appears near and in advance to the phase angle 0° without exception (see Figures 5a, 7a and 7b, and 8a). This means that many earthquakes tend to occur a little before the shear stress in the slip direction attains the maximum. In the case of volumetric stress J1, the peak is found near the phase angle ±180° (maximum compression) for reverse fault type, and near the phase angle 0° (maximum tension) for normal fault type (see Figures 7h, 8b, 9a and 9b).

5. Discussion

[27] In our analysis, we changed the ocean tide model from a conventional model used in past studies including *Tsuruoka et al.* [1995] to a recent one. Figure 10 shows one example of comparison between observed data at the ground surface and theoretical tidal estimates by using these two ocean tide models. The observed data are north-south strain component obtained at DIT station of Tohoku University in the northeastern part of Japan. This station is located at a 20 km distance from the Pacific coastline so that the effect of ocean loading is expected to be very large. From the original observed data, only the tidal components are extracted by using a tidal filtering program, BAYTAP-G [*Tamura et al.*, 1991]. The theoretical curves are also obtained after applying BAYTAP-G, and include both the direct and indirect terms. Figure 10 shows that the theoretical estimate of a recent model (NAO.99b) explains the observed data better than that of a conventional one (Schwiderski), particularly for the period from 7 to 10 September and from 20 to 23 September. Therefore replacing the ocean tide model led to more realistic estimation of the tidal stress at the location of hypocenter. The resolution of analysis was also much improved by using a large number of earthquakes.

[28] The data we used include some earthquake clusters such as aftershocks and earthquake swarms. The existence of clusters may result in an apparent correlation between the Earth tide and earthquake occurrence. To eliminate this effect, we also carried out an analysis by using a declustered earthquake catalog, in which clustered earthquakes were removed using an algorithm of *Reasenberg* [1985]. The number of earthquakes was reduced to 8618 by the declustering. We examined the data subsets classified in the same way as Tables 3–5. As a result of the analysis, we obtained small p values ($p < 5\%$) for all the 11 cases that are indicated in Tables 3–5. Of these 11 cases, the p values for the declustered catalog were smaller for seven cases and larger for the other four cases. Although the observed p values differed a little, we reached the same results for the declustered catalog as those for the original data set. This indicates that the existence of earthquake clusters has little effect on our conclusion.

[29] Through the analysis with higher reliability, we have revealed a significant correlation between the Earth tide and earthquake occurrence using the 9350 globally distributed earthquakes. The correlation was in particular remarkable for the earthquakes of reverse fault type, and high correlation was also found for normal fault type. *Tsuruoka et al.* [1995] examined the 988 global earthquakes, which are also listed in the Harvard CMT catalog, and reported a significant correlation for normal fault type. Since most earthquakes they analyzed were shallow (focal depth < 70 km) and larger (surface wave magnitude ≥ 6.0) ones, their result is consistent with ones for normal fault type earthquakes that we obtained (see Table 6). They also found weak correlation for reverse fault type earthquakes, while clear correlation was found for them in our analysis. Many reverse fault type earthquakes occur near ocean margins, where the effect of ocean loading is very strong; therefore the weaker correlation they obtained may be attributed to lower reliability of the theoretical Earth tide, as was shown in the above discussion.

[30] In our analysis, a high correlation between the Earth tide and earthquake occurrence was not found for strike-slip type in contrast to dip-slip types (reverse and normal fault types). This may be attributed to the difference in the amplitude of tidal stress, since the stress is much smaller in the horizontal direction as compared with the vertical direction. As an example, we compare the tidal shear stress on dip-slip and strike-slip faults at the same location. For the dip angle of fault plane, we use different values for the calculation of stress change; 30° for dip-slip and 90° for strike-slip. The tidal shear stress also varies with the dip angle of fault plane, though its effect is less than that of the slip direction. Typical dip angles depend on fault types as

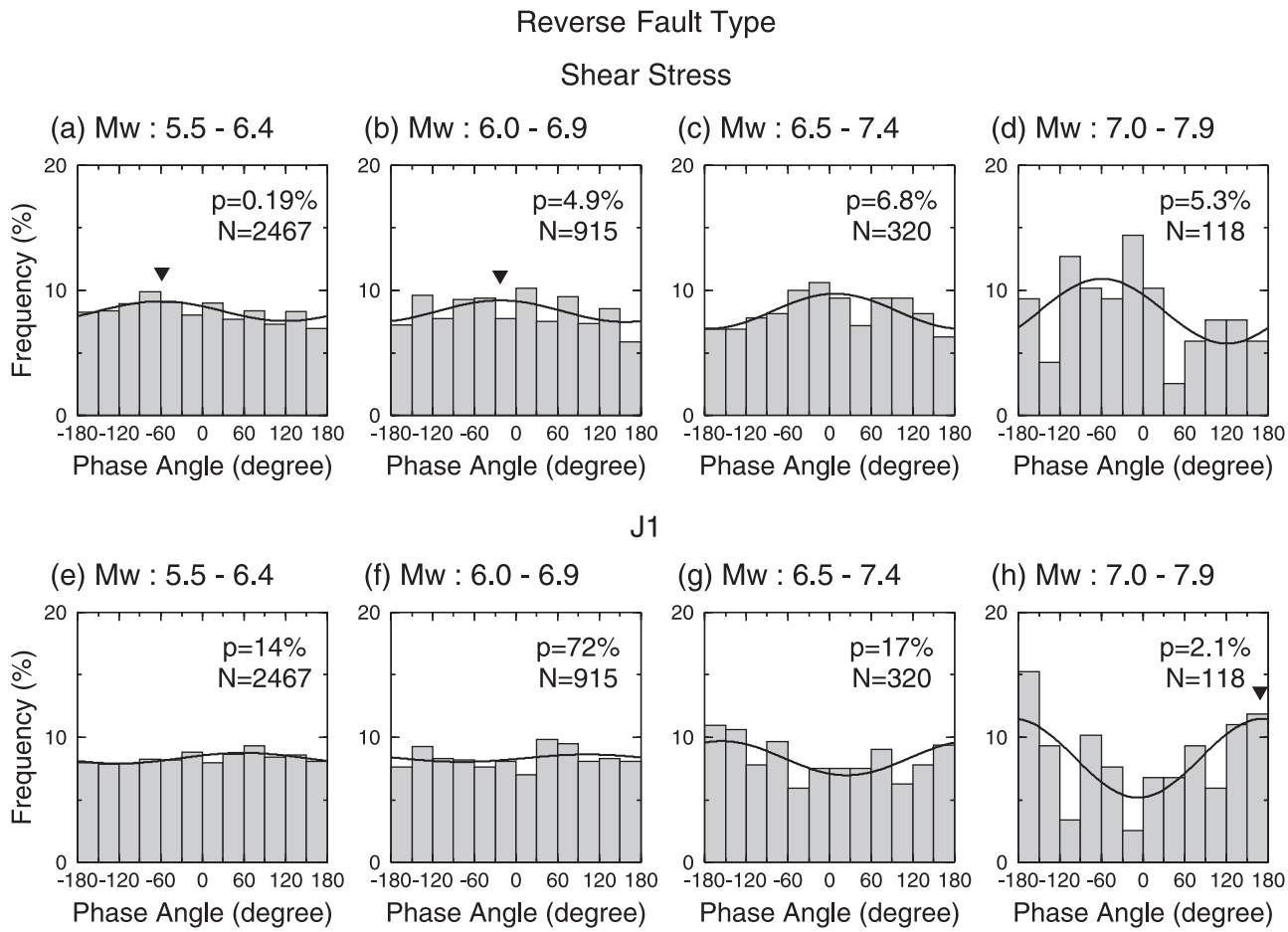

Figure 7. Frequency distributions of tidal phase angles for reverse fault type: (a)–(d) for the shear stress and (e)–(h) for J1. Histograms are shown for four earthquake magnitude ranges: $5.5 \leq M_w \leq 6.4$ (Figures 7a and 7e), $6.0 \leq M_w \leq 6.9$ (Figures 7b and 7f), $6.5 \leq M_w \leq 7.4$ (Figures 7c and 7g), and $7.0 \leq M_w \leq 7.9$ (Figures 7d and 7h). Solid curve represents a sinusoidal function fitted to the distribution, of which peak is indicated by a triangle for the cases of $p < 5\%$.

shown in Figure 11, which shows the frequency distribution of dip angles for the earthquakes used in this study. The Harvard CMT catalog gives two nodal planes, and the histograms are separately shown following to the definition of the first and second nodal planes in the catalog. The distribution is symmetrical for dip-slip faults. We use the average dip angle of the first nodal plane, since the shear stress does not depend on the selection of the nodal plane due to the symmetry of the stress tensor. For strike-slip faults, we use the peak angle of the total frequency including both planes. Figure 12 gives two examples of comparison of the tidal shear stress. Dip-slip and strike-slip faults, which have the above values of dip angle, are located at the same place for each panel; at high latitude (51°N) with east-west strike (Figure 12a) and at low latitude (10°S) with north-south strike (Figure 12b). Parameters used in the calculation are shown in the figure caption. Both examples clearly show that the tidal stress change on dip-slip faults is much larger than that on strike-slip ones.

[31] On the basis of laboratory experiment of stick-slip under periodic loading, *Lockner and Beeler* [1999] reported that the correlation between the loading and the timing of stick-slip events was sensitive to the amplitude of periodic loading; as the amplitude of loading decreased, the correlation also decreased. This result is in good harmony with our inference that absence of a significant correlation for strike-slip type earthquakes may be attributed to smaller amplitude of the tidal stress change. *Vidale et al.* [1998], examining the occurrence time of 13,042 earthquakes in California, reported that earthquakes are randomly distributed throughout the tidal cycle. Since most of the earthquakes they used are strike-slip type, their result is consistent with our finding.

[32] In all the cases of small p values for the shear stress, many earthquakes tend to occur when the stress in the slip direction increases toward its maximum. This indicates that an earthquake may be triggered by the tidal stress accelerating the fault slip. On the other hand, in the cases of small p values for J1, the tidal phase angles of reverse fault type earthquakes distribute with a peak at the maximum compressional stress, while those of normal fault type earthquakes concentrate near the maximum tensional stress. This contrast suggests a close relation between the tidal effect on earthquake occurrence and tectonic regime since reverse and normal faults are associated with the tectonic environments of compressional and tensional horizontal

Table 4. Results of Schuster's Test for Shallow Earthquakes with Various Ranges of Earthquake Magnitude[a]

Mw	*N*	*p*, %	
		Shear Stress	J1
	Reverse Fault		
5.5–6.4	2245	0.68[b]	5.4
6.0–6.9	826	17	17
6.5–7.4	280	21	33
7.0–7.9	104	17	4.2[b]
	Normal Fault		
5.5–6.4	654	7.1	66
6.0–6.9	197	69	2.1[b]
6.5–7.4	55	43	3.8[b]
7.0–7.9	14	26	14
	Strike-Slip Fault		
5.5–6.4	1852	93	14
6.0–6.9	641	98	79
6.5–7.4	145	96	20
7.0–7.9	35	12	23
	Oblique Fault		
5.5–6.4	282	2.2	27
6.0–6.9	64	96	80
6.5–7.4	20	27	9.8
7.0–7.9	4	83	9.9

[a] Focal depth < 70 km.
[b] $p < 5\%$.

stress, respectively. To make it clear, we examine the effect of J1′, the trace of horizontal stress tensor, instead of J1, although J1′ is not an invariant quantity. Figure 13 shows the frequency distribution of phase angles of J1′ for the same data subsets as shown in Figures 7h, 8b, 9a and 9b, all of which indicated small p values for J1. In gross features, the histograms of Figure 13 are quite similar to corresponding ones for J1 although the p values are a little smaller for all the cases. The peak of frequency distribution appears near the maximum of the compressional horizontal stress for reverse fault type (Figures 13a and 13b), and near the maximum of the tensional horizontal stress for normal fault type (Figures 13c and 13d), respectively. This means that earthquake occurrence is encouraged when the tidal stress

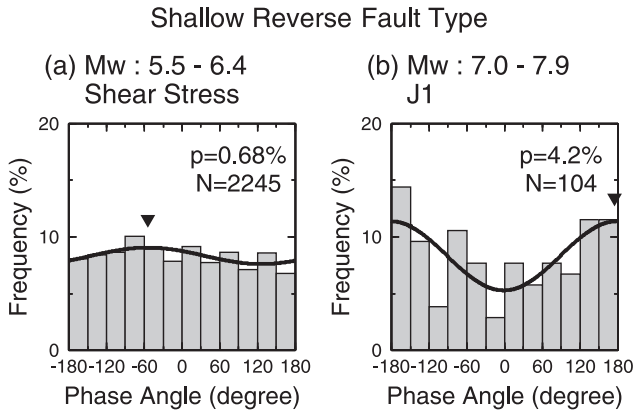

Figure 8. Frequency distributions of tidal phase angles for shallow reverse fault type earthquakes in case of $p < 5\%$: (a) $5.5 \leq M_w \leq 6.4$ for the shear stress, (b) $7.0 \leq M_w \leq 7.9$ for J1. Solid curve represents a sinusoidal function fitted to the distribution, of which peak is indicated by a triangle.

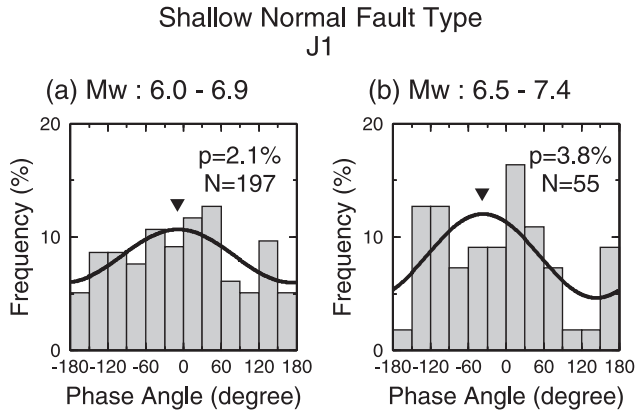

Figure 9. Frequency distributions of tidal phase angles for shallow normal fault type earthquakes in case of $p < 5\%$, J1: (a) $6.0 \leq M_w \leq 6.9$ and (b) $6.5 \leq M_w \leq 7.4$. Solid curve represents a sinusoidal function fitted to the distribution, of which peak is indicated by a triangle.

acts in the same sense as the tectonic stress. Therefore our observation is summarized as that earthquakes tend to concentrate near the phase angle at which the tidal stress accelerates the fault slip both for the shear stress and for the trace of stress tensor. This regularity, being commonly found for all the cases of small p values, indicates that the correlation between the Earth tide and earthquake occurrence we observed is a physical consequence of stress change and cannot be attributed to a stochastic chance.

[33] We found that the correlation between the Earth tide and earthquake occurrence depends on earthquake magni-

Table 5. Results of Schuster's Test for Deep Earthquakes with Various Ranges of Earthquake Magnitude[a]

Mw	*N*	*p*, %	
		Shear Stress	J1
	Reverse Fault		
5.5–6.4	222	16	16
6.0–6.9	89	4.0[b]	0.40[b]
6.5–7.4	40	14	33
7.0–7.9	14	16	33
	Normal Fault		
5.5–6.4	278	77	20
6.0–6.9	110	3.4[b]	57
6.5–7.4	47	9.4	71
7.0–7.9	14	11	9.5
	Strike-Slip Fault		
5.5–6.4	133	58	22
6.0–6.9	35	55	32
6.5–7.4	2	18	23
7.0–7.9	1	37	37
	Oblique Fault		
5.5–6.4	219	28	16
6.0–6.9	62	94	14
6.5–7.4	24	41	74
7.0–7.9	7	62	68

[a] Focal depth ≥ 70 km.
[b] $p < 5\%$.

Table 6. Results of This Study[a]

Fault Type	Depth					
	All		Shallow		Deep	
	Shear Stress	J1	Shear Stress	J1	Shear Stress	J1
Reverse	o[b]	o[c]	o[b]	o[c]	o[b]	o[b]
Normal	×	×	×	o[c]	o[b]	×
Strike-slip	×	×	×	×	×	×
Oblique	×	×	o[b]	×	×	×

[a] A circle indicates the case in which $p < 5\%$ appears for some magnitude range(s), and a cross indicates the other case.
[b] Correlation is remarkable for smaller earthquakes.
[c] Correlation is remarkable for larger earthquakes.

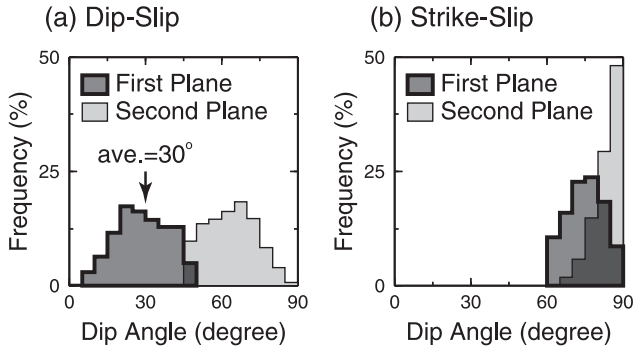

Figure 11. Frequency distributions of dip angles of nodal planes for earthquakes used in this study. Dark and light histograms are for the first and second nodal planes listed in the Harvard CMT catalog, respectively.

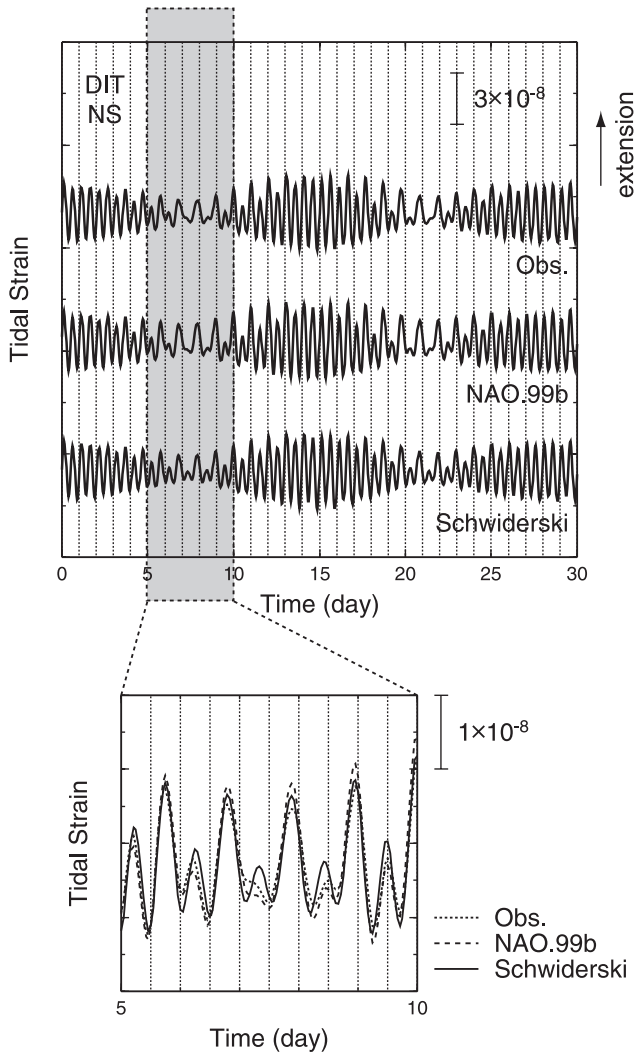

Figure 10. (top) Comparison between the observed and theoretical north-south strain at DIT station (141.4°E, 39.1°N). The period is from 1 to 30 September 1989 (UT). Theoretical curves, including both the direct and indirect terms, are computed by using two ocean tide models; NAO.99b, and *Schwiderski* [1980]. A tidal filter, BAYTAP-G is applied both for the observed and theoretical curves. (bottom) Enlargement of a 5-day portion of the records.

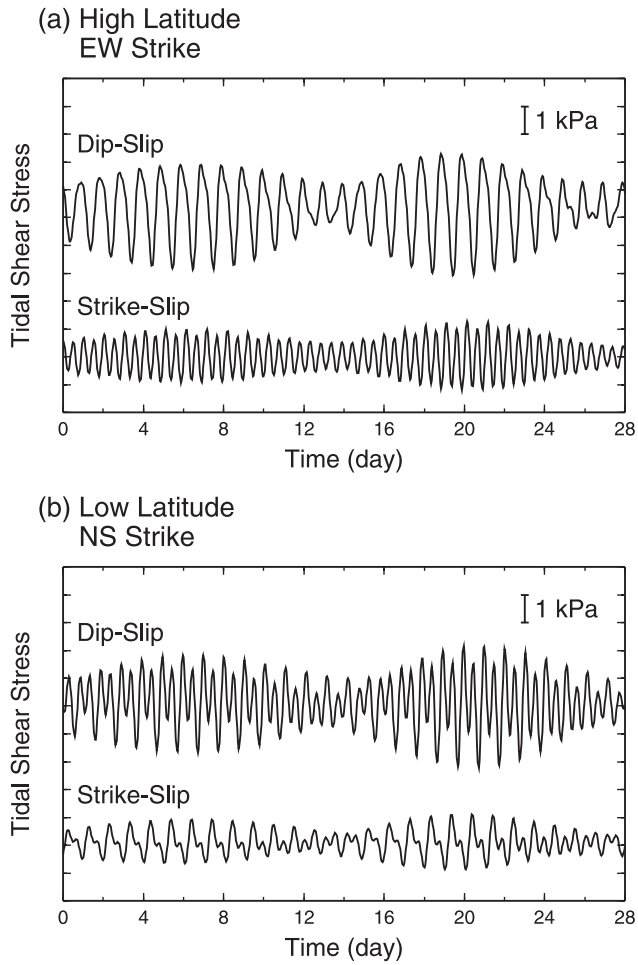

Figure 12. Examples of the tidal shear stress on dip-slip and strike-slip faults at the same location; (a) 180°E, 51°N (strike 270°), (b) 80°W, 10°S (strike 0°). The depth of the faults is set at 15 km. The rake and dip angles are 90° and 30° for dip-slip, and 0° and 90° for strike-slip, respectively. The period is from 1 to 28 January 2000 (UT).

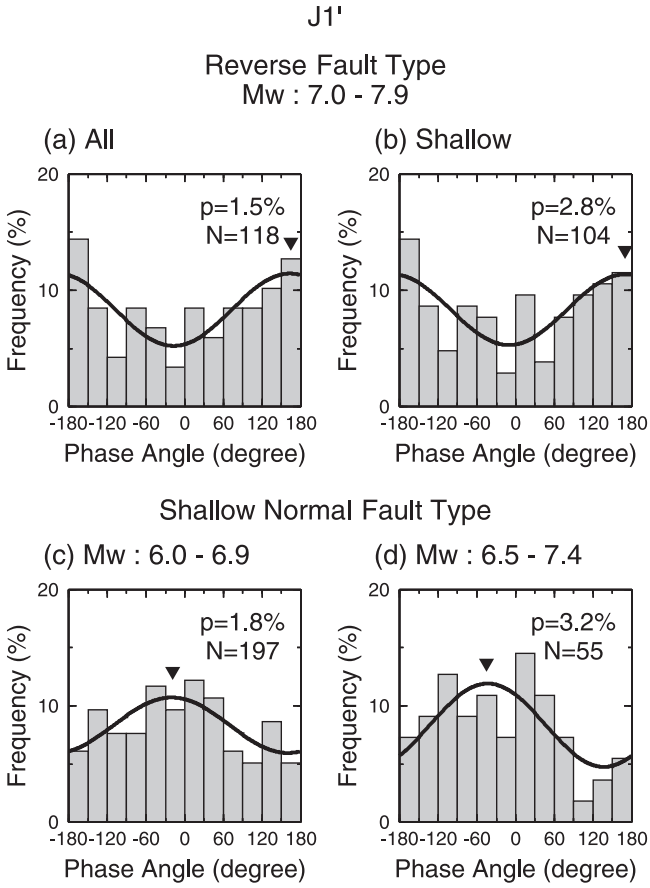

Figure 13. Frequency distributions of tidal phase angles for the trace of horizontal stress tensor, J1′, in case of $p < 5\%$ for J1. (top) Histograms for reverse fault type earthquakes with $7.0 \leq M_w \leq 7.9$: (a) including both shallow and deep earthquakes and (b) only shallow ones. (bottom) Histograms for shallow normal fault type earthquakes: (c) $6.0 \leq M_w \leq 6.9$ and (d) $6.5 \leq M_w \leq 7.4$. Solid curve represents a sinusoidal function fitted to the distribution, of which peak is indicated by a triangle.

tude. It is difficult to clearly interpret this effect, but we briefly discuss some possibilities. First, we used the location of centroid instead of initial rupture point to calculate the tidal stress. As earthquake magnitude becomes larger, the distance between them can be longer. If the tidal stress affects earthquake occurrence, the effect may appear at the initial rupture point. Therefore magnitude dependence on tidal triggering effect may be attributed to the difference between the locations of initial rupture point and centroid. On the other hand, we cannot deny the possibility that a small p value accidentally appeared by excessively dividing the data set. Of course, we also cannot exclude the possibility that the earthquake size dependency may reflect some nature of earthquake occurrence, although we cannot clarify the physical mechanism so far.

[34] As for the stress component of the Earth tide, we focused on the shear stress and the trace of stress tensor, J1. However, the normal stress also affects fault rupture. In order to reveal the normal stress effect, we need to discriminate the fault plane from two nodal planes. This may be possible to some extent for some regions whose tectonics are well known and stable: for example, active fault zones such as the San Andreas fault [*Vidale et al.*, 1998], and typical subduction zones. When the effect of normal stress is clarified, more detailed discussion on the physical mechanism of tidal triggering of earthquakes will become possible from a viewpoint of the Coulomb failure function [e.g., *Jaeger and Cook*, 1969] and laboratory-driven friction laws [e.g., *Dieterich*, 1979].

6. Conclusion

[35] We examined temporal correlation between the Earth tide and earthquake occurrence for 9350 globally distributed earthquakes with magnitude 5.5 or larger, of which locations and focal mechanisms are taken from the Harvard University CMT catalog. The stress due to the Earth tide was theoretically calculated using the PREM Earth model and a recent ocean tide model, NAO.99b. The stress components we examined are the shear stress on the fault plane and the trace of stress tensor, J1. We defined the tidal phase angle for each earthquake and statistically tested whether the phase angles concentrate near some particular angle or not by using the Schuster's method. This test provides p value that indicates the significance level to reject the null hypothesis that earthquakes occur randomly irrespective of the phase angle. For the data set that includes all the earthquakes, no correlation was found both for the shear stress and for J1. However, we found a significant correlation by classifying the data set according to the fault types. The result is summarized as follows:

1. For reverse fault type, an extremely high correlation appears for the shear stress. The correlation is particularly remarkable for shallow and smaller earthquakes. A significant correlation with J1 is also found for larger earthquakes.
2. For normal fault type, a significant correlation with J1 is found for shallow and larger earthquakes.
3. For strike-slip type, no correlation is found.
4. For all the cases of high correlation, earthquake origin times concentrate around the tidal phase angle that accelerates the fault slip, which indicates that high correlation is not accidental but is physically justified.

[36] Those new findings were obtained by a highly reliable analysis that is supported by a recent ocean tide model and large-sized earthquake data set. The result we obtained strongly suggests that a small stress change due to the Earth tide may trigger an earthquake when the stress in the future focal area is close to failure in an earthquake.

[37] **Acknowledgments.** We would like to thank J. E. Vidale and an anonymous reviewer for their helpful comments to the manuscript. We are grateful to K. Matsumoto for making available the ocean tide model, NAO.99b integrated in the computer software GOTIC2. We wish to thank Y. Tamura and M. Ishiguro, who developed the tidal analysis program, BAYTAP-G. We also thank the Research Center for Prediction of Earthquakes and Volcanic Eruptions, Tohoku University for providing us with observed strain data.

References

Alterman, Z., H. Jarosch, and C. L. Pekeris, Oscillations of the earth, *Proc. R. Soc. London, Ser. A*, *252*, 80–95, 1959.

Berg, E., Triggering of the Alaskan earthquake of March 28, 1964, and major aftershocks by low ocean tide loads, *Nature*, *210*, 893–896, 1966.

Curchin, J. M., and W. D. Pennington, Tidal triggering of intermediate and deep focus earthquakes, *J. Geophys. Res.*, *92*, 13,957–13,967, 1987.
Dieterich, J. H., Modeling of rock friction, 1, Experimental results and constitutive equations, *J. Geophys. Res.*, *84*, 2161–2168, 1979.
Ding, Z., J. Jia, and R. Wang, Seismic triggering effect of tidal stress, *Tectonophysics*, *93*, 319–335, 1983.
Dziewonski, A. M., and D. L. Anderson, Preliminary reference Earth model, *Phys. Earth Planet. Inter.*, *25*, 297–356, 1981.
Emter, D., Tidal triggering of earthquakes and volcanic events, in *Tidal Phenomena, Lect. Notes Earth Sci.*, vol. 66, edited by H. Wilhelm, W. Zurn, and H.-G. Wenzel, pp. 293–309, Springer-Verlag, New York, 1997.
Farrell, W. E., Deformation of the Earth by surface loads, *Rev. Geophys.*, *10*, 761–797, 1972.
Hartzell, S., and T. Heaton, The fortnightly tide and the tidal triggering of earthquakes, *Bull. Seismol. Soc. Am.*, *79*, 1282–1286, 1989.
Heaton, T. H., Tidal triggering of earthquakes, *Geophys. J. R. Astron. Soc.*, *43*, 307–326, 1975.
Heaton, T. H., Tidal triggering of earthquakes, *Bull. Seismol. Soc. Am.*, *72*, 2181–2200, 1982.
Jaeger, J. C., and N. G. W. Cook, *Fundamentals of Rock Mechanics*, 513 pp., Methuen, New York, 1969.
Klein, F. W., Earthquake swarms and the semidiurnal solid Earth tide, *Geophys. J. R. Astron. Soc.*, *45*, 245–295, 1976.
Knopoff, L., Earth tides as a triggering mechanism for earthquakes, *Bull. Seismol. Soc. Am.*, *54*, 1865–1870, 1964.
Lockner, D. A., and N. M. Beeler, Premonitory slip and tidal triggering of earthquakes, *J. Geophys. Res.*, *104*, 20,133–20,151, 1999.
Longman, I. M., A green's function for determining the deformation of the earth under surface mass loads, 1, Theory, *J. Geophys. Res.*, *67*, 845–850, 1962.
Matsumoto, K., T. Takanezawa, and M. Ooe, Ocean tide models developed by assimilating TOPEX/POSEIDON altimeter data into hydrodynamical model: A global model and a regional model around Japan, *J. Oceanogr.*, *56*, 567–581, 2000.
Matsumoto, K., T. Sato, T. Takanezasa, and M. Ooe, GOTIC2: A program for computation of oceanic tidal loading effect, *J. Geod. Soc. Jpn.*, *47*, 243–248, 2001.
McNutt, S. R., and R. J. Beavan, Patterns of earthquakes and the effect of solid earth and ocean load tides at Mount St. Helens prior to the May 18, 1980, eruption, *J. Geophys. Res.*, *89*, 3075–3086, 1984.
Mohler, A. S., Earthquake/Earth tide correlation and other features of the Susanville, California, earthquake sequence of June–July 1976, *Bull. Seismol. Soc. Am.*, *70*, 1583–1593, 1980.
Morgan, W. J., J. O. Stoner, and R. H. Dicke, Periodicity of earthquakes and the invariance of the gravitational constant, *J. Geophys. Res.*, *66*, 3831–3843, 1961.
Oike, K., and K. Taniguchi, The relation between seismic activities and Earth tides in the case of the Matsushiro earthquake swarm, *Bull. Disaster Prev. Res. Inst. Univ. Kyoto*, *38*, 17–28, 1988.
Reasenberg, P., Second-order moment of central California seismicity, 1969–1982, *J. Geophys. Res.*, *90*, 5479–5495, 1985.
Ryall, A., J. D. VanWormer, and A. E. Jones, Triggering of microearthquakes by earth tides, and other features of the Truckee, California, earthquake sequence of September, 1966, *Bull. Seismol. Soc. Am.*, *58*, 215–248, 1968.
Rydelek, P. A., P. M. Davis, and R. Y. Koyanagi, Tidal triggering of earthquake swarms at Kilauea Volcano, Hawaii, *J. Geophys. Res.*, *93*, 4401–4411, 1988.
Rykunov, A. L., and V. B. Smirnov, Variations in seismicity under the influences of lunar-solar tidal deformations, *Izv. Acad. Sci. USSR Phys. Solid Earth Ser.*, *21*, 71–75, 1985.
Saito, M., Some problems of static deformation of the Earth, *J. Phys. Earth*, *22*, 123–140, 1974.
Sauck, W. A., The Brawley, California earthquake sequence of January, 1975, and triggering by Earth tides, *Geophys. Res. Lett.*, *2*, 506–509, 1975.
Schuster, A., On lunar and solar periodicities of earthquakes, *Proc. R. Soc. London*, *61*, 455–465, 1897.
Schwiderski, E. W., On charting global ocean tides, *Rev. Geophys.*, *18*, 243–268, 1980.
Shirley, J. H., Lunar and solar periodicities in large earthquakes: Southern California and the Alaska-Aleutian Islands seismic region, *Geophys. J.*, *92*, 403–420, 1988.
Shlien, S., Earthquake-tide correlation, *Geophys. J. R. Astron. Soc.*, *28*, 27–34, 1972.
Shudde, R. H., and D. R. Barr, An analysis of earthquake frequency data, *Bull. Seismol. Soc. Am.*, *67*, 1379–1386, 1977.
Shum, C. K., N. Yu, and C. S. Morris, Recent advances in ocean tidal science, *J. Geod. Soc. Jpn.*, *47*, 528–537, 2001.
Simpson, J. F., Earth tides as a triggering mechanism for earthquakes, *Earth Planet. Sci. Lett.*, *2*, 473–478, 1967.
Souriau, M., A. Souriau, and J. Gagnepain, Modeling and detecting interactions between Earth tides and earthquakes with application to an aftershock sequence in the Pyrenees, *Bull. Seismol. Soc. Am.*, *72*, 165–180, 1982.
Takanezawa, T., K. Matsumoto, M. Ooe, and I. Naito, Effects of the long-period ocean tides on Earth rotation, gravity and crustal deformation predicted by global barotropic model—periods from Mtm to Sa, *J. Geod. Soc. Jpn.*, *47*, 545–550, 2001.
Takeuchi, H., and M. Saito, Seismic surface waves, in *Seismology: Surface Waves and Earth Oscillations, Methods Comput. Phys.*, vol. 11, edited by B. A. Bolt, pp. 217–295, Academic, San Diego, Calif., 1972.
Tamura, Y., T. Sato, M. Ooe, and M. Ishiguro, A procedure for tidal analysis with a Bayesian information criterion, *Geophys. J. Int.*, *104*, 507–516, 1991.
Tsuruoka, H., M. Ohtake, and H. Sato, Statistical test of the tidal triggering of earthquakes: Contribution of the ocean tide loading effect, *Geophys. J. Int.*, *122*, 183–194, 1995.
Ulbrich, U., L. Ahorner, and A. Ebel, Statistical investigations on diurnal and annual periodicity and on tidal triggering of local earthquakes in central Europe, *J. Geophys.*, *61*, 150–157, 1987.
Vidale, J. E., D. C. Agnew, M. J. S. Johnston, and D. H. Oppenheimer, Absence of earthquake correlation with Earth tides: An indication of high preseismic fault stress rate, *J. Geophys. Res.*, *103*, 24,567–24,572, 1998.
Young, D., and W. Zurn, Tidal triggering of earthquakes in the Swabian Jura?, *J. Geophys.*, *45*, 171–182, 1979.

M. Ohtake, H. Sato, and S. Tanaka, Department of Geophysics, Graduate School of Science, Tohoku University, Aoba-ku, Sendai 980-8578, Japan. (ohtake@zisin.geophys.tohoku.ac.jp; sato@zisin.geophys.tohoku.ac.jp; tanaka@zisin.geophys.tohoku.ac.jp)